applied sciences

MDPI

Article

Calculation of Main Circuit Steady-State Parameters for Capacitor Commutated Converter System

Ming Yan, Zheren Zhang * and Zheng Xu

Department of Electrical Engineering, Zhejiang University, No. 38 Zheda Road, Hangzhou 310027, China
* Correspondence: 3071001296zhang@zju.edu.cn

Abstract: The calculation of the main circuit parameters is the basic part of the engineering design for high voltage direct current (HVDC) transmission systems. Compared to the conventional line commutated converter (LCC), the application of the capacitor commutated converter (CCC) can reduce the probability of commutation failures and the shunt capacitor reactive compensation. This paper proposes a calculation method of main circuit parameters for the CCC-based HVDC system. Firstly, the topology of a CCC-HVDC transmission system is described. Secondly, based on the steady-state mathematical model of the CCC, the paper proposes the calculation method of the commutation capacitor to satisfy the system requirements, and the calculation formulas of the main circuit parameters are also given. Then the calculation procedure of the main circuit steady-state parameters is described in detail considering system parameters, control modes, calculation tolerances and operating conditions. Finally, a two-terminal ±500 kV/3000 MW LCC-CCC HVDC transmission system is presented to verify the validity of the main circuit parameter calculation method. The proposed method has great significance for the AC filter design in practical engineering application.

Keywords: main circuit parameter calculation; capacitor commutated converter (CCC); line commutated converter (LCC); LCC-CCC HVDC; calculation procedure

Citation: Yan, M.; Zhang, Z.; Xu, Z. Calculation of Main Circuit Steady-State Parameters for Capacitor Commutated Converter System. *Appl. Sci.* **2023**, *13*, 1171. https://doi.org/10.3390/app13021171

Academic Editors: Federico Barrero and Mario Bermúdez

Received: 8 December 2022
Revised: 7 January 2023
Accepted: 13 January 2023
Published: 15 January 2023

1. Introduction

The high voltage direct current system (HVDC) is currently the main means for long-distance bulk power transmission [1]. In the situation of the bulk power transmission, the line commutated converter (LCC) technology has been widely utilized. When connected to a weak AC grid, the LCC is prone to commutation failures. Moreover, the reactive power consumption of the LCC is 50–60% of the rated DC power. Although the voltage source converter (VSC) can solve most of the above issues, the power rating of this technology still cannot match the LCC.

The concept of using a capacitor commutated converter (CCC) was first proposed in 1954 [2]. It was an alternative technology to the LCC and has the potential to mitigate the above drawbacks of the LCC. The series capacitors are inserted between the valve side of converter transformers and the thyristor valves to generate an additional commutation voltage. The world's first commercial CCC-HVDC project was the Garabi Project in 2000, which allowed power transmission from an Argentina network (50 Hz) to a Brazilian network (60 Hz) with a very low short circuit ratio (SCR) at the Brazilian side [3]. In 2003, the CCC technology was also chosen for Rapid City DC Tie to realize the seventh asynchronous interconnection between the eastern and western networks in North America [4]. As one of the longest transmission links in the world, the Rio Madeira Project was commissioned in 2013–2014. A part of the project was the 800 MW back-to-back CCC-HVDC that provided power in the weaker power networks of northwest Brazil [5,6]. The CCC technology was selected for these three projects due to its suitability for application in relatively weak systems. Compared to the conventional LCC, the application of the CCC can reduce the

probability of commutation failures and is suitable for the weak AC systems. Moreover, it can reduce the shunt capacitor reactive compensation from AC filters [7].

The calculation of the main circuit parameters is essential to the design of the HVDC transmission system, which provides the steady-state operation parameters for the filter design and the calculation of harmonics. The main circuit parameter calculation aims to determine the steady-state operation characteristics (e.g., firing angle, extinction angle and ideal no-load DC voltage), steady-state parameters of the converter transformers and reactive power compensation [1]. Before further investigating the features of the CCC, it is necessary to propose a design method to calculate the main circuit parameters of the CCC-HVDC transmission system. The design methods of the main circuit parameters for the LCC, modular multilevel converter (MMC), multiterminal LCC-HVDC, multiterminal MMC-HVDC and M3C are already demonstrated in [8–13].

With the fixed series capacitor insertions, the CCC not only increases the AC harmonics but also represents additional valve voltage stress. Moreover, the unbalanced commutation voltages of the capacitors under fault conditions may lead to the transient performance deterioration [14]. To improve the controllability of the inserted capacitors, Reference [15] introduces an approach to the CCC using an active capacitor. A three-phase voltage sourced converter (VSC) is connected to resemble the effect of the capacitor. In [16], a small-rated three-phase VSC is added between the series commutation capacitor and the thyristor-based converter in CCC. The series VSC acts as an auxiliary commutation capacitor to actively change the series capacitance and mitigate the continuous commutation failure (CF) issue of the CCC. The evolved capacitor commutated converter (ECCC), embedded with anti-parallel thyristor-based dual-directional full-bridge modules is proposed in [17], which can effectively reduce CF risks. An improved coordinated control strategy for ECCC was proposed in [18] to accelerate the commutation process under normal operation state and further reduce the CF probability under AC fault conditions. In [2], the fully controlled insulated gate bipolar transistor (IGBT) submodules (SMs) are used to form the full-bridge capacitor module. This novel hybrid converter configuration aims to eliminate commutation failures under serious faults. To effectively alleviate the limitation of IGBTs for ultra HVDC systems, Reference [19] proposes an approach using a thyristor based controllable capacitor (TBCC) to eliminate CF and reduce the loss from the power devices. Reference [20] proposes a control strategy for a hybrid HVDC system comprising a CCC connected in series with a two-stage VSC. Reference [21] gives a literature review about the mitigation of the commutation failure. The CCC technology is one of the improvements to converters, which focus on the topological structure of the entire converter. The series capacitor is considered in [22] with the capacitance selection factors. However, the detailed CCC system model is not derived.

For a CCC, the series capacitors are inserted between the valve side of converter transformers and the thyristor valves to realize the elimination of the commutation failure when connected to the weak AC system. This CCC technology is economical and easy to realize, which has potential in the future engineering application. However, the above researches mainly focus on the topology improvement for the CCC to further enhance the transient characteristics during the commutation failure. The main circuit parameters of the CCC are directly given and the design method is not even mentioned in these studies. Thus, this paper systematically provides a design method of the main circuit parameters, which is beneficial for the further research of the CCC. The contribution of this paper is as follows:

(1) The calculation method of the commutation capacitor in a six-pulse CCC is proposed in this paper. Firstly, the waveform of the commutation capacitors is depicted in detail. Then the commutation process is derived to obtain a steady-state mathematical model of the CCC. After applying the proposed selection principles (the limitations of the valve stress and the reactive power consumption), the value of the commutation capacitor is determined.

(2) The design method and the detailed calculation procedure of the main circuit parameters for a two-terminal LCC-CCC HVDC transmission system are proposed in this paper. The calculation formulas of the operation parameters at both converter sides are presented. The paper also gives a modified Guizhou–Guangdong II ±500 kV/3000 MW LCC-CCC HVDC transmission system to verify the validity of the proposed calculation method. The simulation and calculation results are compared to further illustrate the features of the CCC.

The organization of this paper is as follows. In Section 2, the topology of a ±500 kV/3000 MW LCC-CCC HVDC transmission system is proposed. In Section 3, the steady-state mathematical model of the CCC is presented and the calculation formulas of the main circuit parameters are given. In Section 4, the basic factors required for the main circuit parameter calculation are explained and a detailed calculation procedure is given. In Section 5, a case study under a certain operating condition is presented to verify the validity of the proposed calculation method. A simulation in PSCAD/EMTDC is carried out to reflect the characteristics of the CCC and give a comparison between the experimental and calculation results. Finally, conclusions are drawn in Section 6.

2. Topology of the LCC-CCC HVDC

The LCC-CCC HVDC transmission system studied in this paper is constructed by modifying the inverter of a conventional two-terminal LCC-HVDC transmission system. The modified system adopts the conventional LCC at the rectifier side and the CCC at the inverter side, which is shown in Figure 1. Series capacitors are inserted between the converter transformer and the thyristor valves in each phase at the inverter side.

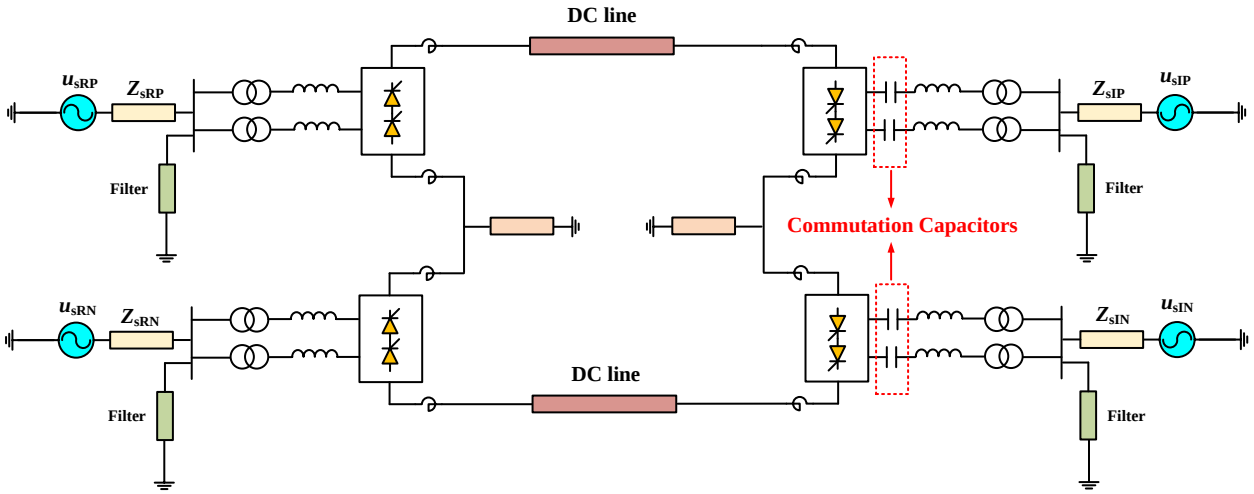

Figure 1. Topology of the two-terminal LCC-CCC HVDC transmission system.

The rated voltage and power transmission capacity of the LCC-CCC HVDC transmission system in this paper are chosen as ±500 kV/3000 MW. Both converters adopt the operation of the bipolar twelve-pulse valve group. The length of DC power transmission line is 1150 km.

3. Calculation Model and Method of the Main Circuit Parameters

In this section, the CCC at the inverter side is explained in detail firstly. Then the voltage waveform of the commutation capacitor is drawn and the commutation process of the CCC is derived to give the steady-state mathematical model of the CCC. After applying the proposed selection principles (the limitations of the valve stress and the reactive power consumption), the value of the commutation capacitor is determined. Finally, the calculation formulas of the main circuit parameters at both sides are given. Thus, the theoretical analysis of the LCC-CCC HVDC system is completed.

3.1. Determination of the Capacitance Value

For a CCC, capacitors are inserted between the converter transformer and thyristor valves. Thus, the determination of the capacitance value is important for the main circuit parameter design. To analyze the characteristics of the CCC, a six-pulse CCC equivalent model at the inverter side is arranged in Figure 2.

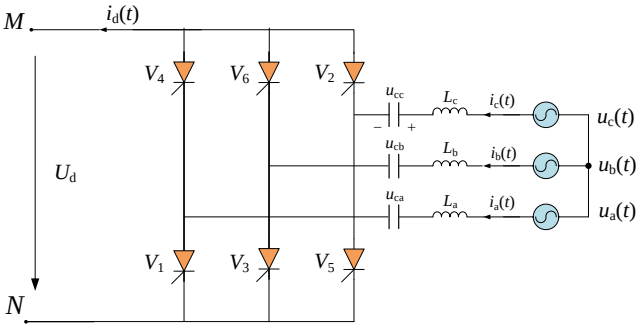

Figure 2. Diagram of a six-pulse CCC equivalent model at the inverter side.

The grid side voltage is converted to the valve side voltage with the help of converter transformers. Considering the smoothing reactor at the DC side, it is assumed that the DC current remains unchanged for the steady-state calculation. The valve side voltage and the capacitor voltage are vector superimposed to obtain the commutation voltage, whose amplitude is greater than that of the conventional LCC under the same conditions.

3.1.1. Voltage Waveform of Commutation Capacitors

The voltage waveforms of the commutation capacitors for a six-pulse CCC are shown in Figure 3. The three-phase capacitor voltages u_{ca}, u_{cb} and u_{cc} present periodic changes. To further explore the voltage change in the capacitor in the commutation process and the non-commutation process, the commutation capacitor voltage waveforms of phase A in Figure 3 is partially enlarged, as shown in Figure 4.

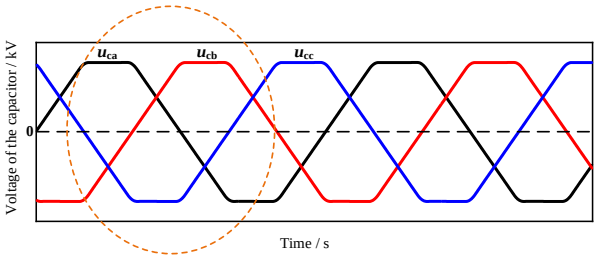

Figure 3. Voltage waveforms of the commutation capacitors.

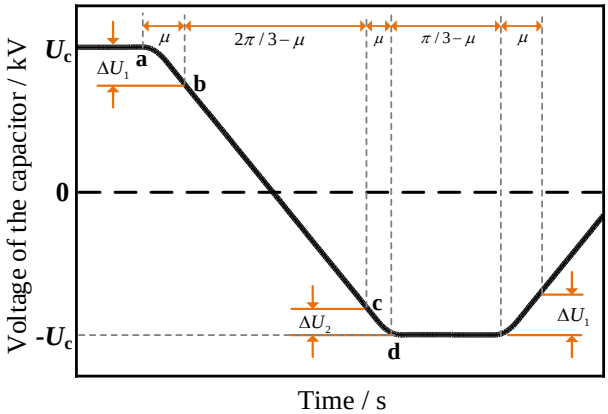

Figure 4. Partially enlarged voltage waveform of the commutation capacitor in phase A.

In Figure 4, curve ab represents the commutation process from valve 2 to valve 4, and the corresponding capacitor voltage drops from U_c to $U_c - \Delta U_1$. Straight line bc indicates that only valve 4 is on at the common anode. The commutation capacitor of phase A discharges from $U_c - \Delta U_1$ to 0, and reversely charges from 0 to $\Delta U_2 - U_c$. Curve cd represents the commutation process from valve 4 to valve 6, and the corresponding capacitor voltage drops from $\Delta U_2 - U_c$ to $-U_c$. ΔU_1 and ΔU_2 represent the voltage change in the commutation capacitor connected in series with the phase entering the commutation and the phase exiting the commutation during the commutation process. ΔU_1 and ΔU_2 can be calculated as follows:

$$\Delta U_1 = \left| \frac{1}{\omega C} \int_{\alpha}^{\alpha+\mu} i_k d\theta \right| \tag{1}$$

$$\Delta U_2 = \left| \frac{1}{\omega C} \int_{\alpha}^{\alpha+\mu} [(-1)^{k+1} I_d - i_k] d\theta \right| \tag{2}$$

where i_k is the commutation current of the k-th commutation process, α is the firing angle and μ is the overlap angle.

The peak capacitor voltage U_c satisfies:

$$2U_c = \Delta U_1 + (\frac{2\pi}{3} - \mu)\frac{I_d}{\omega C} + \Delta U_2 \tag{3}$$

3.1.2. Steady-State Mathematical Model of the CCC

Taking the trigger of valve 1 as an example, the instantaneous line-to-neutral AC source voltages are:

$$\begin{cases} u_a = \frac{\sqrt{2}}{\sqrt{3}} E \sin(\omega t + \alpha + \frac{\pi}{6}) \\ u_b = \frac{\sqrt{2}}{\sqrt{3}} E \sin(\omega t + \alpha - \frac{\pi}{2}) \\ u_c = \frac{\sqrt{2}}{\sqrt{3}} E \sin(\omega t + \alpha + \frac{5\pi}{6}) \end{cases} \tag{4}$$

where E is the root mean square (rms) value of the line-to-line voltage at the valve side.

In the interval $[0, \mu]$, valve 5 is commutated to valve 1 and valve 6 is on. The equivalent circuit of the converter is shown in Figure 5.

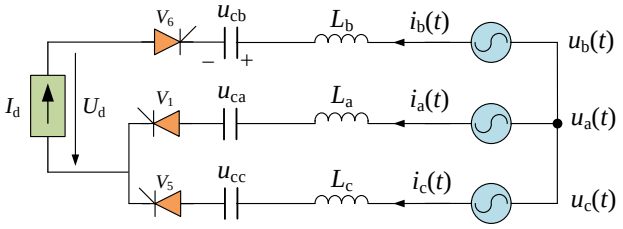

Figure 5. Equivalent circuit of the commutation process in the interval $[0, \mu]$.

According to Kirchhoff's current law, the currents satisfies:

$$i_a + i_c = I_d \tag{5}$$

Integrate both sides of (5) to obtain:

$$\frac{1}{\omega C}\int_0^{\mu} i_a d\theta + \frac{1}{\omega C}\int_0^{\mu} i_c d\theta = \frac{1}{\omega C}\int_0^{\mu} I_d d\theta \tag{6}$$

According to (1) and (2), the relationship between ΔU_1 and ΔU_2 is:

$$\Delta U_1 + \Delta U_2 = \frac{\mu I_d}{\omega C} \tag{7}$$

Substituting (7) into (3), the peak capacitor voltage U_c is:

$$U_c = \frac{\pi I_d}{3\omega C} \tag{8}$$

According to Kirchhoff's voltage law, the differential equation of the commutation process can be derived as:

$$u_a(t) - u_c(t) = L_a \frac{di_a}{dt} + u_{ca}(t) - L_c \frac{di_c}{dt} - u_{cc}(t) \tag{9}$$

Differentiate both sides of (9) to obtain:

$$\frac{d^2 i_a}{dt^2} + \frac{1}{LC} i_a = \frac{1}{2LC} I_d + \frac{1}{2L}\left(u_a'(t) - u_c'(t)\right) \tag{10}$$

The solution of (10) is:

$$i_a(t) = A\cos(\omega_0 t) + B\sin(\omega_0 t) + \frac{1}{2} I_d + \frac{\sqrt{2}\omega}{2L(\omega_0^2 - \omega^2)} E\cos(\omega t + \alpha) \tag{11}$$

where ω_0 is the angular frequency of oscillation during the commutation process, satisfying:

$$\omega_0 = \sqrt{1/LC} \tag{12}$$

The boundary conditions are:

$$\begin{cases} i_a(\omega t = 0) = 0 \\ i_a(\omega t = \mu) = I_d \end{cases} \tag{13}$$

Substitute (13) into (11) to obtain:

$$A + \frac{1}{2} I_d + \frac{\sqrt{2}\omega}{2L(\omega_0^2 - \omega^2)} E\cos\alpha = 0 \tag{14}$$

$$A\cos(\frac{\omega_0}{\omega}\mu) + B\sin(\frac{\omega_0}{\omega}\mu) - \frac{1}{2} I_d + \frac{\sqrt{2}\omega}{2L(\omega_0^2 - \omega^2)} E\cos(\mu + \alpha) = 0 \tag{15}$$

When ωt = 0, substitute (11) into (9) to obtain:

$$\frac{1}{2L}(\frac{2\pi I_d}{3\omega C} - \Delta U_2) - B\omega_0 + \frac{\sqrt{2}\omega_0^2}{2L(\omega_0^2 - \omega^2)} E\sin\alpha = 0 \tag{16}$$

When ωt = μ, substitute (11) into (9) to obtain:

$$\frac{1}{2L}(\frac{2\pi I_d}{3\omega C} - \Delta U_1) + A\omega_0\sin(\frac{\omega_0}{\omega}\mu) - B\omega_0\cos(\frac{\omega_0}{\omega}\mu) + \frac{\sqrt{2}\omega_0^2}{2L(\omega_0^2 - \omega^2)}\frac{\sqrt{2}}{\sqrt{3}} E\sin(\mu + \alpha) = 0 \tag{17}$$

The DC voltage of the six-pulse CCC is:

$$u_d = \begin{cases} -\frac{1}{2}u_a - \frac{1}{2}u_c + u_b - \frac{3\Delta U_2}{2} + \frac{3\theta I_d}{2\omega C} & \theta \in (0, \mu) \\ -u_a + u_b - \frac{\pi I_d}{3\omega C} - 2\Delta U_2 + \frac{2\theta I_d}{\omega C} & \theta \in (\mu, \frac{\pi}{3}) \end{cases} \tag{18}$$

The average value of the DC voltage over a period is:

$$U_d = \frac{3}{\pi}(\int_0^{\mu} u_d d\theta + \int_{\mu}^{\pi/3} u_d d\theta) \tag{19}$$

Substitute (18) into (19) to obtain:

$$U_d = -\frac{3\sqrt{2}}{2\pi}E[\cos\alpha + \cos(\alpha+\mu)] + (1-\frac{3\mu}{4\pi})(\Delta U_1 - \Delta U_2) \tag{20}$$

In the CCC, the apparent extinction angle γ_{app} is defined as the electrical angle corresponding to the time at which the valve turns off to the positive zero-crossing of the line-to-line voltage at the AC valve side [23]. It is easily obtained that the firing angle, the overlap angle and the apparent extinction angle in each period add up to π.

$$\alpha + \mu + \gamma_{app} = \pi \tag{21}$$

The real extinction angle γ_{real} is defined as the electrical angle corresponding to the time at which the valve turns off to the positive zero-crossing of the line-to-line commutation voltage. The commutation voltage lags the valve side voltage due to the voltage drop across the series commutation capacitor. Thus, the real extinction angle γ_{real} is larger than the apparent extinction angle γ_{app}. When $\omega t = \mu + \gamma_{real}$, the voltage drop across the valve 5 is 0, satisfying:

$$v_5 = (u_c - u_{cc}) - (u_a - u_{ca}) = 0 \tag{22}$$

The corresponding boundary conditions are:

$$u_{cc} = \frac{\pi I_d}{3\omega C} \quad , \quad u_{ca} = \frac{\gamma_{real} I_d}{\omega C} + \Delta U_1 - \frac{\pi I_d}{3\omega C} \tag{23}$$

Substitute (23) into (22) to obtain:

$$\sqrt{2}E\sin(\alpha+\mu+\gamma_{real}) + (\frac{2\pi}{3} - \gamma_{real})\frac{I_d}{\omega C} - \Delta U_1 = 0 \tag{24}$$

In addition, the power characteristics of the CCC are the same as those of the conventional LCC. Thus, the active power and reactive power can be described as:

$$P_d = U_d I_d \tag{25}$$

$$Q_d = P_d \frac{\sin(2\gamma_{app}) - \sin(2\gamma_{app}+2\mu) + 2\mu}{\cos(2\gamma_{app}) - \cos(2\gamma_{app}+2\mu)} \tag{26}$$

The commutation inductance is derived as:

$$L = \frac{u_k E}{\sqrt{2}\omega I_d} \tag{27}$$

where u_k is the short-circuit impedance of the converter transformer, which is available from the equipment instruction.

According to the equivalent circuit of the CCC, the peak voltage across the valves [24] can be derived as:

$$u_{VTmaxCCC} = \sqrt{2}E\sin(\frac{\pi}{3} + \gamma_{app}) + \frac{\pi I_d}{3\omega C} + \Delta U_1 \tag{28}$$

Equations (7), (12), (14)–(17), (20), (21), (24)–(28) constitute the steady-state mathematical model of the six-pulse CCC.

There are 15 state variables in the above equations, including γ_{real}, μ, α, ΔU_1, ΔU_2, A, B, P_d, Q_d, γ_{app}, C, ω_0, L, E, $u_{VTmaxCCC}$. However, only 13 equations are available. If any two of these state variables are determined, the rest of the state variables can also be calculated.

3.1.3. Selection Principles of the Commutation Capacitor

From the above analysis, it is important to determine the value of the two state variables before determining the commutation capacitor. The selection principles are as follows:

- Principle 1: The valve stress of a CCC is limited typically 10% higher than that of a conventional LCC [25].
- Principle 2: The total reactive power consumption is defined as 15% of the rated DC power [26].

For Principle 1, the insertion of the commutation capacitor will add the additional voltage stress on valve thyristors. When selecting the capacitance value, the peak voltage across the valves of the CCC is 1.1 times that of the LCC under the same conditions, which can meet the design requirements. Therefore, the state variable $u_{VTmaxCCC}$ is determined.

For Principle 2, once Q_d is determined as 15% of the rated DC power, the consumption of the total reactive power is diminished as compared to about 50% in the case of the conventional LCC. Thus, the insertion of the commutation capacitor can reduce the amount of devices for the reactive power compensation and improve the power factor at the AC side.

When system parameters of the CCC are determined, $u_{VTmaxCCC}$ and Q_d can be calculated. The equations in Section 3.1.2 can be solved by MATLAB to obtain the unique solution and the capacitance value can also be determined.

3.2. Calculation Formulas of Main Circuit Parameters

In this section, the formulas used for calculation of the main parameters at both converter sides are presented. The rectifier side adopts the conventional LCC and the inverter side adopts the CCC.

3.2.1. Calculation of the DC Voltages

The formula for calculating the DC voltage across the six-pulse rectifier is:

$$U_{dR} = U_{dioR}[\cos\alpha - (d_{xR} + d_{rR})\frac{I_d}{I_{dN}}\frac{U_{dioNR}}{U_{dioR}}] - U_T \tag{29}$$

The DC voltage of the six-pulse inverter U_{dI} is calculated according to (20).

For the monopolar ground return mode, the voltage U_{dR} and U_{dI} can also be calculated from the system point of view:

$$\begin{cases} U_{dR} = U_{dLR} + (R_{eR} + R_{gR})I_d \\ U_{dI} = U_{dLI} - (R_{eI} + R_{gI})I_d \end{cases} \tag{30}$$

For the bipolar mode, the voltage is:

$$\begin{cases} U_{dR} = U_{dLR} \\ U_{dI} = U_{dLI} \end{cases} \tag{31}$$

where U_T is the forward voltage drop of the LCC. U_{dLR} and U_{dLI} are the pole to ground DC voltages at the rectifier side and the inverter side, respectively. U_{dioR} is the ideal no-load DC voltage of the six-pulse rectifier and U_{dioRN} is the rated ideal no-load DC voltage of the six-pulse rectifier. I_d is the DC current and I_{dN} is the rated DC current. d_{xR} and d_{rR} are the relative inductive voltage drop and the relative resistive voltage drop, respectively. R_{eR} and R_{eI} are the resistances of the rectifier and inverter electrode line, respectively. R_{gR} and R_{gI} are the resistances of the rectifier and inverter electrode, respectively. α is the firing angle at the rectifier side.

3.2.2. Calculation of the DC Voltage Difference

The pole to ground voltage difference ΔU between the rectifier and the inverter is defined as:

$$\Delta U = U_{\mathrm{dLR}} - U_{\mathrm{dLI}} = R_{\mathrm{d}} I_{\mathrm{d}} \tag{32}$$

where R_{d} is the DC line resistance on the pole level.

For the monopolar ground return mode, the relationship between U_{dR} and U_{dI} is:

$$U_{\mathrm{dR}} - U_{\mathrm{dI}} = U_{\mathrm{dLR}} - U_{\mathrm{dLI}} + (R_{\mathrm{eR}} + R_{\mathrm{gR}} + R_{\mathrm{eI}} + R_{\mathrm{gI}}) I_{\mathrm{d}} \tag{33}$$

For the monopolar metallic return mode, the relationship is:

$$U_{\mathrm{dR}} - U_{\mathrm{dI}} = 2R_{\mathrm{d}} I_{\mathrm{d}} \tag{34}$$

For the bipolar mode, the relationship is:

$$U_{\mathrm{dR}} - U_{\mathrm{dI}} = U_{\mathrm{dLR}} - U_{\mathrm{dLI}} \tag{35}$$

3.2.3. Calculation of the Rated Relative Inductive and Resistive Voltage Drops

The rated relative inductive voltage drop determines the short-circuit current value of the thyristor valve. It is defined as:

$$d_{\mathrm{xRN}} = \frac{3}{\pi} \frac{X_{\mathrm{t}} I_{\mathrm{dN}}}{U_{\mathrm{dioN}}} \approx (u_{\mathrm{k}} + \text{relative voltage drop in PLC filter reactors})/2 \tag{36}$$

where X_{t} is the commutation reactance.

In practical engineering, the rated relative resistive voltage drop d_{rRN} is generally taken as 0.3%.

3.2.4. Calculation of the Overlap Angles

The overlap angle of the rectifier μ_{R} can be calculated according to:

$$\cos(\alpha + \mu_{\mathrm{R}}) = \cos\alpha - 2d_{\mathrm{xRN}} \frac{I_{\mathrm{d}}}{I_{\mathrm{dN}}} \frac{U_{\mathrm{dioNR}}}{U_{\mathrm{dioR}}} \tag{37}$$

The overlap angle of the inverter μ_{I} can be derived from the steady-state mathematical model of the CCC in Section 3.1.

3.2.5. Calculation of the Reactive Power Consumptions

The reactive power consumption at the rectifier side Q_{dR} can be calculated as:

$$Q_{\mathrm{dR}} = P_{\mathrm{dR}} \frac{\sin(2\alpha) - \sin(2\alpha + 2\mu_{\mathrm{R}}) + 2\mu_{\mathrm{R}}}{\cos(2\alpha) - \cos(2\alpha + 2\mu_{\mathrm{R}})} \tag{38}$$

The reactive power consumption at the inverter side Q_{dI} can be calculated according to (26).

3.2.6. Calculation of the Voltage and Current at the Valve Side

The AC voltage at the valve side is:

$$U_{\mathrm{v}} = \frac{U_{\mathrm{dio}}}{\sqrt{2}} \frac{\pi}{3} \tag{39}$$

The AC current at the valve side is:

$$I_{\mathrm{v}} = \sqrt{\frac{2}{3}} I_{\mathrm{d}} \tag{40}$$

3.2.7. Calculation of the Rated Power of the Converter Transformer

The total rated three-phase power of the six-pulse converter transformer is:

$$S_{\text{transN}} = \sqrt{3} U_{\text{vN}} I_{\text{vN}} = \frac{\pi}{3} U_{\text{dioN}} I_{\text{dN}} \tag{41}$$

where I_{vN} and U_{vN} are the rated AC current and voltage at the valve side, respectively.

3.2.8. Calculation of the Converter Transformer Tap

The range of the converter transformer tap is mainly determined by the steady-state fluctuation range of the AC bus voltage, the operation mode of the HVDC transmission system, the reduced DC voltage operation level, the power limit transmitted under the reduced DC voltage operation mode and the maximum allowable control angle of the thyristor valve.

In the rated operation mode, the rated tap of the converter transformer corresponds to the '0' gear. The rated transformation ratio can be calculated as follows:

$$\eta_{\text{nom}} = \frac{U_{1\text{N}}}{U_{\text{vN}}} = \frac{U_{1\text{N}}}{\frac{U_{\text{dioN}}}{\sqrt{2}} \frac{\pi}{3}} \tag{42}$$

When calculating the on-load tap range of the converter transformer, the maximum and minimum transformation ratio can be calculated as follows:

$$\eta_{\text{max}} = \frac{U_{1\text{max}} U_{\text{dioN}}}{U_{1\text{N}} U_{\text{diominOLTC}}} \tag{43}$$

$$\eta_{\text{min}} = \frac{U_{1\text{min}} U_{\text{dioN}}}{U_{1\text{N}} U_{\text{diomaxOLTC}}} \tag{44}$$

where $U_{1\text{N}}$, $U_{1\text{max}}$, $U_{1\text{min}}$ are the rated value, maximum value and minimum value of the grid side AC voltage of the converter transformer, respectively. U_{vN} is the rated value of the valve side AC voltage. $U_{\text{diomaxOLTC}}$ and $U_{\text{diominOLTC}}$ are the maximum and minimum no-load DC voltage for equipment selection, respectively.

The on-load tap changer of the converter transformer can be calculated according to:

$$TC = \frac{\eta - 1}{\Delta\eta} \tag{45}$$

where $\Delta\eta$ is the one on-load tap changer step, which is taken as 1.25%.

Therefore, the maximum and minimum on-load tap changers of the converter transformer are:

$$+TC = \frac{\eta_{\text{max}} - 1}{\Delta\eta} \tag{46}$$

$$-TC = \frac{\eta_{\text{min}} - 1}{\Delta\eta} \tag{47}$$

It can be seen that the number of positive and negative taps is determined according to the steady-state variation range of the grid side AC voltage and the extreme value of the no-load DC voltage at the valve side. However, the result calculated by the above formula only meets the the minimum requirements. The calculation of the maximum on-load tap changer also needs to consider the 70% reduced DC voltage operation. In addition, the degree of the DC voltage drop is related to the control angle of the converter.

4. Calculation Procedure of Main Circuit Parameters

The design of the main circuit parameters aims to calculate all the steady-state characteristics of the rectifier and the inverter considering the control modes of converters and transformers. Usually, the calculation results of the main circuit parameters mainly include the following parameters: the DC power, the DC voltage, the DC current, the firing angle at the rectifier side, the extinction angle at the inverter side, the overlap angle, the reactive power consumed by the converter, the voltage of the valve side and the on-load tap changer of the converter transformer.

This subsection firstly discusses the basic factors required for the main circuit parameter design of the proposed CCC system, including the system parameters, the control modes, the restriction conditions and the operating conditions. Then, a detailed calculation procedure is proposed considering these basic factors. Finally, a flow chart is drawn to provide an intuitive procedure of the main circuit parameter design.

4.1. Basic Factors

4.1.1. System Parameters

The system parameters mainly include: the rated DC current I_{dN}, the rated DC voltage U_{dN}, the rated DC resistance R_{dN}, the rated firing angle of the rectifier side α_N, the rated apparent extinction angle at the inverter side γ_{appN}, the rated real extinction angle at the inverter side γ_{realN}, the relative inductive voltage drop d_{xR} and d_{xI}, and the relative resistive drop d_{rR} and d_{rI}.

4.1.2. Control Modes

The LCC at the rectifier side adopts the constant current control and the CCC at the inverter side adopts the constant voltage control. The on-load converter transformers adopt the angle control mode.

The tap control is one of the main control modes to adjust the DC voltage during steady-state operation. There are usually two control modes. One is the voltage control mode, in which the DC voltage or the AC voltage at the valve side is constant. Another is the angle control mode, which keeps the firing angle or the extinction angle within the given range. These two control modes both have applications in practical engineering. The latter requires a wider range of tap changers but can maintain a high power factor under various operating conditions. The angle control mode is the preferred operation control mode for HVDC transmission systems [27] and is adopted in this paper.

4.1.3. Restriction Conditions

The restriction conditions mainly include the minimum value of the firing angle and the extinction angle, the tap changer range of the converter transformer and the minimum reactive power consumption constraint for each converter station.

4.1.4. Operating Conditions

The calculation of the operating conditions needs to consider factors such as the operating configuration, the power transmission direction, the DC voltage level, the DC circuit resistance and the AC system voltage levels at both sides. The typical operating conditions are shown in Table 1.

Table 1. Summary of technical characteristics of various schemes.

Factors for Operating Condition	Classification of the Factor
Operating configuration	Bipolar mode (B) Monopolar ground return mode (G) Monopolar metallic return mode (M)
Power transmission direction	Forward direction (F) Reverse direction (R)
DC voltage level	Full voltage operation (F) 80% reduced voltage operation (R) 70% reduced voltage operation (S)
DC circuit resistance	High resistance (H) Low resistance (L)
AC system voltage level at the rectifier and the inverter side	Maximum rated voltage Nominal voltage Minimum rated voltage Maximum extreme voltage Minimum extreme voltage

4.2. Detailed Calculation Procedure

Under the specific control modes of the converters and the transformers, the design of the main circuit parameters is to determine all steady-state operating parameter values from the minimum DC power (0.1 pu) to the maximum DC power (1.2 pu) with a certain step (0.05 pu).

For an LCC-CCC HVDC transmission system with the LCC at the rectifier side and the CCC at the inverter side, the detailed calculation procedure of the main circuit parameters is as follows:

Step 1: According to Section 3.1, the steady-state mathematical model of the six-pulse CCC at the inverter side is firstly calculated. The capacitance value and the inductance value are determined. The effective value of the line voltage is considered as the rated line voltage at the valve side U_{acNI}. The result of the apparent extinction angle is considered as the rated apparent extinction angle γ_{appN}.

Step 2: Calculate the rated ideal no-load DC voltage U_{dioNR} at the rectifier side and U_{dioNI} at the inverter side:

$$U_{\mathrm{dioNR}} = \frac{(\frac{U_{\mathrm{dNR}}}{p} + U_{\mathrm{T}})}{\cos\alpha_{\mathrm{N}} - (d_{\mathrm{xR}} + d_{\mathrm{rR}})} \tag{48}$$

$$U_{\mathrm{dioNI}} = \frac{3\sqrt{2}}{\pi} U_{\mathrm{acNI}} \tag{49}$$

where U_{acNI} is the rated line voltage at the valve side of the inverter. p is the number of six-pulse valve groups per pole. U_{T} is the forward voltage drop of a six-pulse valve group. U_{dNR} and U_{dNI} represent the rated DC voltage at the rectifier side and the inverter side, respectively, and the relationship satisfies:

$$U_{\mathrm{dNI}} = U_{\mathrm{dNR}} - I_{\mathrm{dN}} R_{\mathrm{d}} \tag{50}$$

Step 3: Design the tap range of the converter transformer and determine the maximum and minimum on-load tap changers of the converter transformer at both sides.

The DC power ranges from the minimum value (0.1 pu) to the maximum value (1.2 pu) with a certain step (0.05 pu). For each step of the DC power, Step 4~Step 13 are executed.

Step 4: Calculate the DC current I_{d} from the DC voltage U_{dR} and the DC power P_{dR} at the rectifier side:

$$I_{\mathrm{d}} = P_{\mathrm{dR}} / U_{\mathrm{dR}} \tag{51}$$

Step 5: For the rectifier, the default tap position of the converter transformer is set at the highest position. At the highest position, the corresponding firing angle and the reactive power consumption are smaller. Thus, the valve stress is reduced and the harmonic currents are diminished, which is beneficial for security and stability.

For the certain tap position, U_{dioR} is calculated as follows:

$$U_{\mathrm{dioR}} = \frac{U_{\mathrm{dioNR}}}{1 + n_{\mathrm{TR}} \cdot \Delta\eta} \frac{U_{\mathrm{acR}}}{U_{\mathrm{acNR}}} \tag{52}$$

where n_{TR} is the tap position of the converter transformer at the rectifier side. U_{acR} is the AC voltage at the rectifier side and U_{acNR} is the rated AC voltage at the rectifier side.

Step 6: Calculate the firing angle α at the rectifier side:

$$\alpha = \arccos\left[\frac{\frac{U_{\mathrm{dR}}}{p} + U_{\mathrm{T}} + (d_{\mathrm{xR}} + d_{\mathrm{rR}}) \cdot \frac{I_{\mathrm{d}}}{I_{\mathrm{dN}}} \cdot U_{\mathrm{dioNR}}}{U_{\mathrm{dioR}}}\right] \tag{53}$$

Step 7: Assuming that the firing angle range is α_{Tmin}~α_{Tmax}, update the tap position n_{TR} according to the calculated α.

- If α is in this range, go to the next Step.
- If $\alpha < \alpha_{\mathrm{Tmin}}$, since α is negatively correlated with n_{TR}, reduce n_{TR} and recalculate α until α is within the specified range. If n_{TR} decreases to the minimum value, there is still $\alpha < \alpha_{\mathrm{Tmin}}$, then set $\alpha = \alpha_{\mathrm{Tmin}}$, solve the Equations (51) and (53) to obtain I_{d} and U_{dR}.

Step 8: According to n_{TR} and Equation (52), update U_{dioR}. Calculate the overlap angle μ_{R} and the reactive power consumption Q_{R} at the rectifier side.

$$\mu_{\mathrm{R}} = \arccos(\cos\alpha - 2 \cdot d_{\mathrm{xR}} \cdot \frac{I_{\mathrm{d}}}{I_{\mathrm{dN}}} \cdot \frac{U_{\mathrm{dioNR}}}{U_{\mathrm{dioR}}}) - \alpha \tag{54}$$

$$Q_{\mathrm{R}} = P_{\mathrm{dR}} \frac{\sin(2\alpha) - \sin(2\alpha + 2\mu_{\mathrm{R}}) + 2\mu_{\mathrm{R}}}{\cos(2\alpha) - \cos(2\alpha + 2\mu_{\mathrm{R}})} \tag{55}$$

Step 9: For the inverter, the default tap position of the converter transformer is set at the highest position. The corresponding AC voltage at the valve side of the CCC is:

$$U_{\mathrm{acI}} = \frac{U_{\mathrm{acNI}}}{1 + n_{\mathrm{TI}} \cdot \Delta\eta} \tag{56}$$

Step 10: Substitute U_{acI} into the steady-state mathematical model of the CCC to calculate γ_{app}, γ_{real}, μ_{I}, P_{I} and Q_{I}.

Step 11: Assume that the extinction angle range satisfies:

$$\begin{cases} \gamma_{\mathrm{app}} \geq \gamma_{\mathrm{appmin}} \\ \gamma_{\mathrm{real}} \geq \gamma_{\mathrm{realmin}} \end{cases} \tag{57}$$

To ensure the commutation margin, set $\gamma_{\mathrm{realmin}} = 17^{\circ}$ and $\gamma_{\mathrm{appmin}} = \gamma_{\mathrm{appN}}$.

If $\gamma_{\mathrm{app}} < \gamma_{\mathrm{appmin}}$ or $\gamma_{\mathrm{real}} < \gamma_{\mathrm{realmin}}$, reduce n_{TI} and recalculate U_{acI}. Then, return to Step 9 to recalculate γ_{app} and γ_{real} until the extinction angles are within the specified ranges.

If n_{TI} is reduced to the minimum value, and γ_{app} (or γ_{real}) is still not within the constraints, then set $\gamma_{\mathrm{app}} = \gamma_{\mathrm{appmin}}$ (or $\gamma_{\mathrm{real}} = \gamma_{\mathrm{realmin}}$). The operating parameters of the rectifier are now determined by those of the inverter. The calculating process is as follows:

Substitute γ_{app} (or γ_{real}) into the steady-state mathematical model of the CCC to calculate the inverter side DC voltage U_{dI}. Calculate the DC voltage U_{dR} according to (58) and update the DC current I_{d} according to (51). Then repeat the calculation to modify U_{dI}, U_{dR} and I_{d}. After several iterations, the accurate U_{dI}, U_{dR} and I_{d} can be obtained.

Finally, update the other operating parameters of the rectifier and the inverter by executing Step 4~Step 10.

$$U_{dR} = U_{dI} + I_d R_d \tag{58}$$

Step 12: Verify whether the reactive power consumption of the rectifier meets the requirements of the minimum reactive power consumption Q_{Rmin}. The purpose is to avoid injecting too much reactive power into the AC system when the DC system is low loaded, especially under the minimum filter control mode. If $Q_R \geq Q_{Rmin}$, go to the next Step, otherwise set $Q_R = Q_{Rmin}$ and recalculate the steady-state parameters at both sides.

Step 13: Verify whether the reactive power consumption of the inverter meets the requirements of the minimum reactive power consumption Q_{Imin}. If $Q_I \geq Q_{Imin}$, go to the next Step, otherwise set $Q_I = Q_{Imin}$ and recalculate the steady-state parameters of both sides.

Step 14: Verify whether each DC power level has been calculated. If so, the calculation of the main circuit parameters is completed. Otherwise, the calculation of the next DC power level is executed.

To further reflect the interaction among the parameters used in the calculation procedure, the target main circuit parameters and the intermediate parameters are summarized in Table 2.

Table 2. The summary of the parameters during the calculation procedure.

	Name of the Parameters	Symbol of the Parameters
Target main circuit parameters	DC power	P_{dR} and P_{dI}
	DC voltage	U_{dR} and U_{dI}
	DC current	I_d
	Firing angle	α
	Extinction angle	γ_{app} and γ_{real}
	Overlap angle	μ_R and μ_I
	Reactive power	Q_R and Q_I
	On-load tap changer of the converter transformer	n_{TR} and n_{TI}
Intermediate parameters	Rated AC line voltage	U_{acNR} and U_{acNI}
	AC line voltage	U_{acR} and U_{acI}
	Rated ideal no-load DC voltage	U_{dioNR} and U_{dioNI}
	Ideal no-load DC voltage	U_{dioR} and U_{dioI}
	Minimum firing angle	α_{Tmin}
	Minimum apparent extinction angle	γ_{appmin}
	Minimum real extinction angle	$\gamma_{realmin}$
	Minimum reactive power consumption	Q_{Rmin} and Q_{Imin}

4.3. Flow Chart of the Main Circuit Parameter Design

The corresponding flow chart is shown in Figure 6. To illustrate the calculation procedure more clearly and specifically, the detailed steps are labelled in every flow chat box.

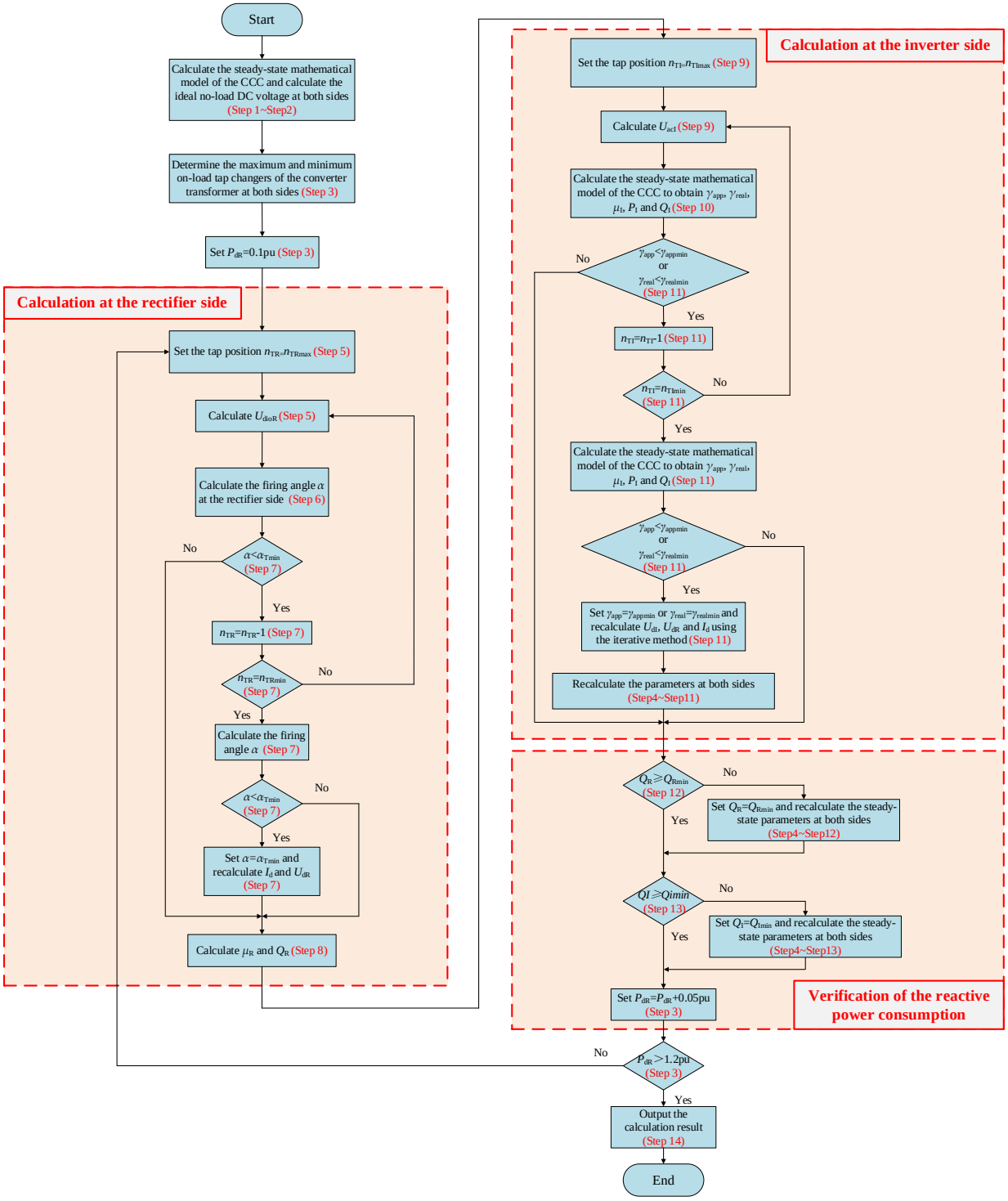

Figure 6. Flow chart of the detailed procedure for the main circuit parameter design.

5. Case Study

In this section, the modified Guizhou–Guangdong II ±500 kV/3000 MW LCC-CCC HVDC transmission system is presented to verify the validity of the main circuit parameter calculation method. The simulation in PSCAD/EMTDC is carried out to reflect the operation of the LCC-CCC HVDC system and show a comparison between the calculation result and the experimental result.

The conventional LCC at the rectifier side adopts the constant DC current control and the CCC at the inverter side adopts the constant DC voltage control. The angle control mode is adopted for the converter transformers at both sides. The operating condition is under bipolar mode, forward direction, full voltage operation, high resistance and normal AC voltages. The system parameters and the converter parameters are shown in Tables 3 and 4, respectively. The rated apparent extinction angle is chosen as 1.57° and the commutation capacitor is chosen as 129.75 μF from the steady-state mathematical model of the CCC in Section 3.1.2.

Table 3. System parameters of the LCC-CCC HVDC transmission system.

System Parameters	Value
Bipolar rated DC power/MW	3000
Rated DC current/kA	3
Rated DC voltage/kV	500
DC line resistance/Ω	10.4
System frequency/Hz	50

Table 4. Converter parameters of the LCC-CCC HVDC transmission system.

Converter Parameters	Value	
	LCC at Rectifier	CCC at Inverter
Rated angle/° [1]	15	1.57
Minimum angle of the transformer angle control mode/°	12.5	1.57
Maximum angle of the transformer angle control mode/°	17.5	/
Rated AC voltage/kV	525	525
Minimum reactive power consumption of the converter/Mvar	140	0
Commutation capacitor/μF	/	129.75

[1] Rated firing angle for the rectifier and rated apparent extinction angle for the inverter.

Considering various measurement errors, the equipment manufacture tolerance and the adjustment range of control parameters (e.g., firing/extinction angle), the calculation results of the converter transformer parameters at both side are shown in Table 5. Due to the commutation capacitors, the ideal no-load DC voltage of the CCC is smaller than that of the LCC.

Table 5. Main parameters of the converter transformer.

Main Parameters	Value	
	LCC at Rectifier	CCC at Inverter
Rated ideal no-load DC voltage U_{dioN}/kV	283.49	237.02
Maximum ideal no-load DC voltage U_{diomax}/kV	286.77	243.27
Minimum ideal no-load DC voltage U_{diomin}/kV	259.33	203.82
Nominal ratio	525/209.92	525/175.51
Tap changer range	−5 to 24	−6 to 32

Following the calculation procedure in Section 4, the calculation results of the main circuit parameters at the rectifier side and the inverter side are shown in Tables 6 and 7, respectively.

Table 6. Main circuit parameters at the rectifier side (data per pole).

P_{dR}/MW	U_{dR}/kV	I_d/kA	α/°	μ_R/°	Q_R/Mvar	Tap
150	317.9	0.472	41.64	2.75	140	24
225	369.2	0.609	29.55	4.59	140	24
300	393.9	0.762	21.25	7.2	140	24
375	406.9	0.922	14.66	10.71	140	24
450	500	0.9	12.6	9.83	145.9	6
525	500	1.05	14.31	10.26	189.8	5
600	500	1.2	13.25	11.88	215.7	5
675	500	1.35	14.92	12.12	266.4	4
750	500	1.5	13.92	13.63	294.6	4
825	500	1.65	12.84	15.2	322.34	4
900	500	1.8	14.6	15.16	382.1	3
975	500	1.95	13.59	16.63	412	3
1050	500	2.1	15.3	16.51	477.9	2
1125	500	2.25	14.35	17.89	509.9	2
1200	500	2.4	13.33	19.33	541.4	2
1275	500	2.55	15.12	19.02	615.8	1
1350	500	2.7	14.16	20.37	649.4	1
1425	500	2.85	13.14	21.78	682.4	1
1500	500	3	15	21.3	765.3	0
1575	500	3.15	14.05	22.62	800.4	0
1650	500	3.3	13.04	24	835	0
1725	500	3.45	14.95	23.38	926.3	−1
1800	500	3.6	14.01	24.67	962.9	−1

Table 7. Main circuit parameters at the inverter side (data per pole).

P_{dI}/MW	U_{dI}/kV	I_d/kA	γ_{app}/°	γ_{real}/°	μ_I/°	Q_I/Mvar	Tap
147.7	313	0.472	20.48	26.48	3.72	60.8	32
221.1	362.9	0.609	11.95	19.4	5.45	58.6	21
294	386	0.762	8.57	17.54	6.76	63.9	16
366.2	397.3	0.922	9.12	19.43	7.12	84.6	13
441.6	490.6	0.9	10.77	18.96	5.98	109.9	−5
513.5	489.1	1.05	7.36	17.17	7.36	104	−4
585	487.5	1.2	8.14	19.13	7.56	127.8	−4
656	486	1.35	8.88	21	7.75	153.1	−4
726.6	484.4	1.5	5.28	19.13	9.08	134.8	−3
796.7	482.8	1.65	6.3	21.22	9.07	161.5	−3
866.3	481.3	1.8	1.88	18.71	10.66	129.7	−2
935.5	479.7	1.95	3.38	21.2	10.39	158.5	−2
1004.1	478.2	2.1	4.63	23.42	10.23	188.5	−2
1072.4	476.6	2.25	5.72	25.46	10.14	219.6	−1
1140.1	475	2.4	1.58	23.31	11.44	175.9	−1
1207.4	473.5	2.55	3.07	25.67	11.16	209.4	−1
1274.2	471.9	2.7	4.34	27.78	10.97	243.9	−1
1340.5	470.4	2.85	5.45	29.71	10.84	279.2	−1
1406.4	468.8	3	1.57	27.94	11.91	225	0
1471.8	467.2	3.15	3.04	30.13	11.65	263.1	0
1536.7	465.7	3.3	4.3	32.1	11.47	301.9	0
1601.2	464.1	3.45	5.4	33.91	11.34	341.2	0
1665.2	462.6	3.6	1.81	32.49	12.21	278.1	1

With the DC power changes from 0.1 pu to 1.2 pu, the firing angle/extinction angle, the DC voltage, the reactive power consumption and the tap position are shown in Figure 7.

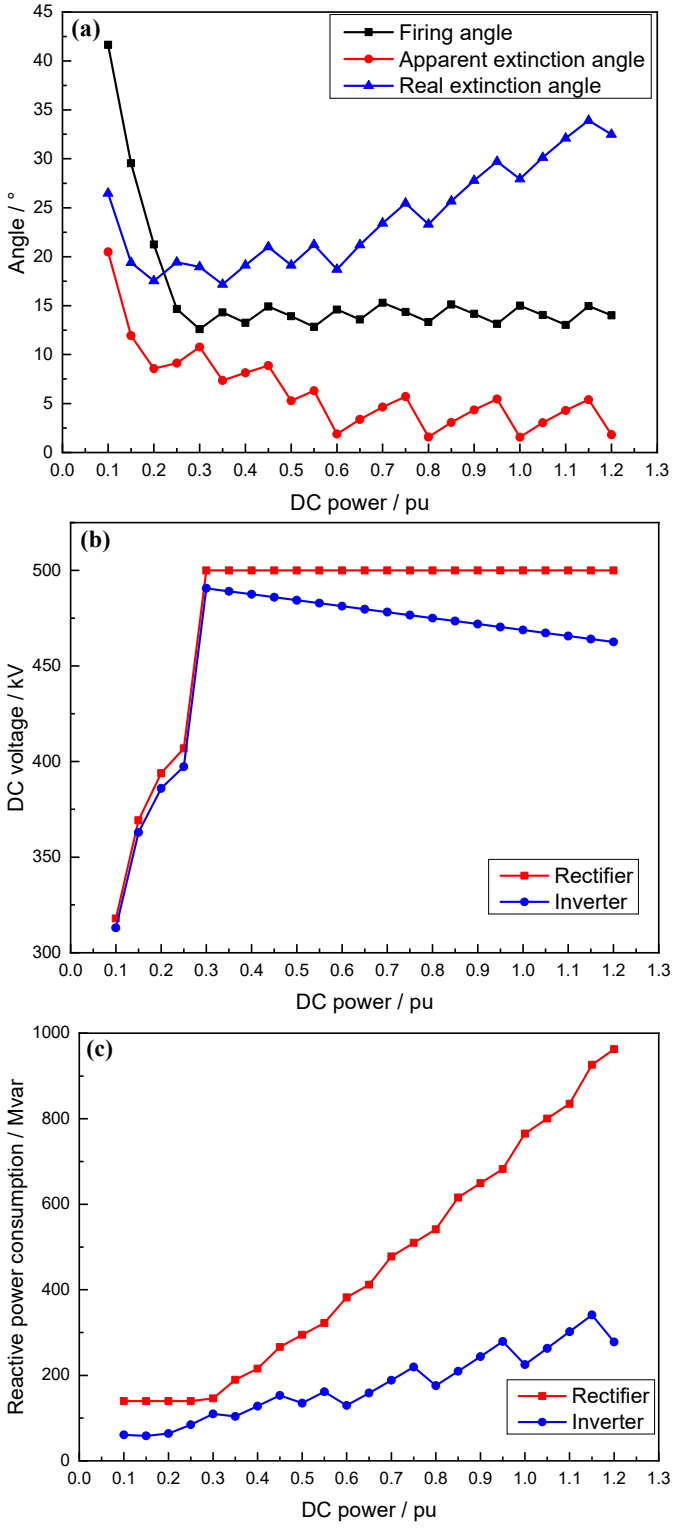

Figure 7. *Cont.*

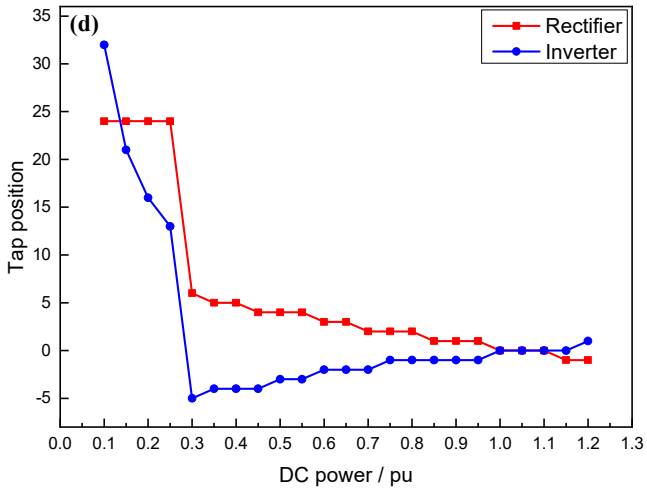

Figure 7. Relationships between some main circuit parameters and the DC power: (**a**) relationship between the angles and the DC power, (**b**) relationship between the DC voltage and the DC power, (**c**) relationship between the reactive power consumption and the DC power, (**d**) relationship between the tap position and the DC power.

Based on the above calculation results, the following conclusions can be drawn:

- Due to the existence of the DC resistance, the DC voltage of the rectifier is always greater than that of the inverter. The voltage difference becomes larger as the DC power increases.
- An appropriate increase in the number of the on-load tap changers will be beneficial to the decrease in the firing angle at the rectifier and the extinction angle at the inverter, thus lowering the consumption of the reactive powers.
- At the low DC power level, due to the restriction of the minimum filter control mode at the rectifier side, the LCC operates under a larger firing angle and the CCC operates under a larger apparent extinction angle. Thus, the reactive power consumptions of both sides will increase. Meanwhile, the DC voltage is below the rated value and the tap changers of the converter transformer are at the higher position.

The model of a ±500 kV/3000 MW LCC-CCC HVDC transmission system (by modifying the Guizhou–Guangdong II ±500 kV/3000 MW LCC-HVDC) is established in PSCAD/EMTDC when the DC power is selected as 1.0 pu. To better illustrate the features of the CCC, the simulation and calculation results of the CCC at the inverter side are shown in Table 8. The simulation results of the conventional LCC at the inverter side are also presented.

The results obtained show that the relative errors between the calculation and the simulation results are within 5%. The CCC consumes less reactive power than the conventional LCC under the same conditions. To further display the characteristics of the thyristor valves, waveforms of the valve voltages and the valve currents are shown in Figures 8 and 9, respectively.

The results show that the peak voltage across the valves of the CCC is about 1.1 times that of the LCC, which can also be seen in Table 8. Due to the extra commutation voltage provided by the commutation capacitors, the voltage stress across the valves of the CCC lags that of the LCC, which will reduce the apparent extinction angle of the CCC and diminish the reactive power consumption. Moreover, the thyristor valve currents of the CCC exhibit larger fluctuations than those of the LCC during the commutation process.

Table 8. Comparison of the simulation and calculation results (DC power is selected as 1.0 pu).

Parameters	Calculation Values of the CCC	Simulation Values of the CCC	Simulation Values of the Conventional LCC [2]	Relative Error between Calculation and Simulation of the CCC	Relative Error between CCC and LCC from Simulations
DC voltage/kV	468.8	479.5	482.2	2.23%	0.56%
DC current/kA	3	3	3	/	/
Active power/MW	1406.4	1438	1447	2.20%	0.62%
Reactive power consumption/Mvar	225	230	816	2.17%	/
Extinction angle/°	1.57	1.571	17	0.06%	/
Peak voltage across the valves/kV	303.4	318.8	289.2	4.83%	10.24%
Peak capacitor voltage/kV	77.07	76.85	/	0.29%	/

[2] The conventional LCC is the inverter of the original Guizhou–Guangdong II ±500 kV/3000 MW HVDC transmission system.

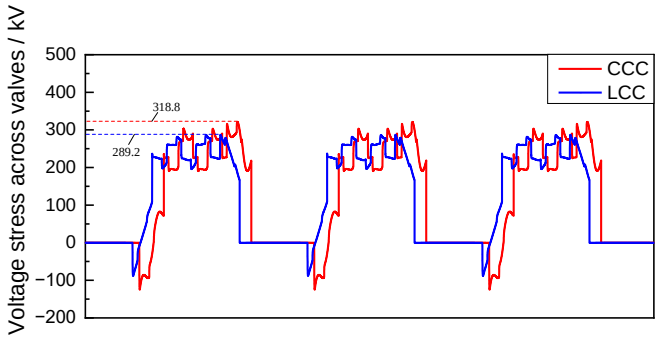

Figure 8. Comparison of the voltage stress across thyristor valves between the CCC and the LCC.

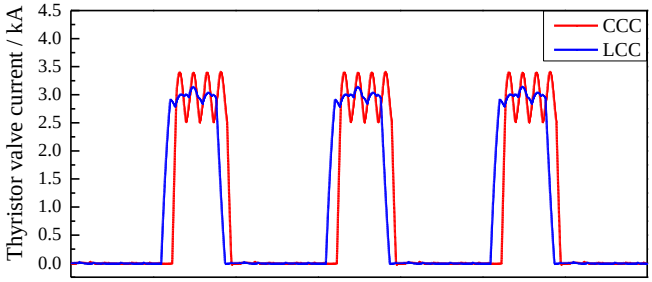

Figure 9. Comparison of the thyristor valve currents between the CCC and the LCC.

6. Conclusions

This paper proposes a calculation method of the commutation capacitor with two selection principles (the limitations of the valve stress and the reactive power consumption). Moreover, relevant formulas of the main circuit parameters for a two-terminal LCC-CCC HVDC transmission system are presented. The detailed calculation procedure is also given. A case study is carried out and the relative errors between the simulation and calculation results are within 5%, which is acceptable for main circuit parameter design. The verification result shows that the apparent extinction angle is always smaller than the real extinction angle, which is caused by the extra commutation voltage provided by the commutation capacitor. Thus, the CCC consumes less reactive power than the conventional LCC due to the smaller extinction angle. The proposed calculation method of the main

circuit parameters will provide guidance for AC filter design, and steady-state and transient analysis of the CCC in further research.

Author Contributions: Conceptualization, Z.X.; methodology, Z.Z.; validation, M.Y.; resources, Z.X., Z.Z. and M.Y.; writing—original draft, M.Y.; writing—review and editing, Z.X. and Z.Z.; visualization, M.Y. All authors have read and agreed to the published version of the manuscript.

Funding: The research has received no external funding.

Institutional Review Board Statement: Not applicable.

Informed Consent Statement: Not applicable.

Data Availability Statement: The data that support the findings of this study are available from the corresponding author upon reasonable request.

Conflicts of Interest: The authors of the paper have no conflict of interest to disclose.

References

1. Xiao, H.; Sun, K.; Pan, J.; Li, Y.; Liu, Y. Review of hybrid HVDC systems combining line communicated converter and voltage source converter. *Int. J. Electr. Power Energy Syst.* **2021**, *129*, 106713. [CrossRef]
2. Xue, Y.; Zhang, X.; Yang, C. Elimination of commutation failures of LCC HVDC System with controllable capacitors. *IEEE Trans. Power Syst.* **2016**, *31*, 3289–3299. [CrossRef]
3. Ottosson, N.; Kjellin, L. Modular back-to-back HVDC with capacitor commutated converters (CCC). In Proceedings of the 7th International Conference on AC-DC Power Transmission, London, UK, 28–30 November 2001; pp. 55–59.
4. Stoltz, M.; Bahrman, M.; Dickinson, D.; Abrahamsson, B. The Rapid City DC Tie. In Proceedings of the 2006 IEEE PES Power Systems Conference and Exposition, Atlanta, GA, USA, 29 October–1 November 2006; pp. 476–479.
5. Graham, J.; Holmgren, T.; Fischer, P.; Shore, N.L. The Rio Madeira HVDC system—Design aspects of bipole 1 and the connector to acre-rondonia. In Proceedings of the CIGRE 2012, Paris, France, 26–31 August 2012.
6. Pinto, M.; Pagioro, A.; Azevedo, R. The Rio Madeira HVDC system—Implementation and commissioning of bipole 1 and the connector to acrerondonia. In *Colloquium, HVDC and Power Electronics to Boost Network Performance, Proceedings of the CIGRE 2013, Brasilia, Brazil, 2–3 October 2013*; ResearchGate: Berlin, Germany, 2013.
7. Kaur, J.; Chaudhuri, N. Analytical modelling of point-to-point CCC-HVDC revisited. *IET Gener. Transm. Distrib.* **2019**, *13*, 916–926. [CrossRef]
8. Wang, F.; Zhang, J. The calculation of main circuit steady state parameters for HVDC system. In Proceedings of the 2009 IEEE/PES Power Systems Conference and Exposition, Seattle, WA, USA, 15–18 March 2009; pp. 1–5.
9. Xu, Z.; Xiao, H.; Zhang, Z. Selection methods of main circuit parameters for modular multilevel converters. *IET Renew. Power Gener.* **2016**, *10*, 788–797. [CrossRef]
10. Han, X.; Li, Y.; Sun, J.; Zhang, Z.; Xu, Z.; Xu, Y. DC Side Main Circuit Parameter Selection of MMC-MTDC Systems with HVDC CBs and SFCLs. In Proceedings of the 2018 International Conference on Power System Technology (POWERCON), Guangzhou, China, 6–8 November 2018; pp. 2313–2318.
11. Yu, S.; Wen, J.; Li, J.; Liu, H. Calculation of main circuit steady state parameters for S-MTDC transmission systems. *J. Eng.* **2019**, *2019*, 1715–1720. [CrossRef]
12. Wang, L.; Wu, F.; Li, D.; Xue, Y. Study on the calculation of main circuit parameters of multi-terminal HVDC transmission systems. In Proceedings of the 16th IET International Conference on AC and DC Power Transmission (ACDC 2020), Online Conference, 2–3 July 2020; pp. 198–204.
13. Ni, X.; Qiu, P.; Lin, J.; Lu, Y.; Jin, Y.; Xu, H. Selection Methods of Main Circuit Parameters for Modular Multilevel Matrix Converters. In Proceedings of the 2021 International Conference on Power System Technology (POWERCON), Haikou, China, 8–9 December 2021; pp. 1304–1309.
14. Hou, L.; Zhang, S.; Wei, Y.; Zhao, B.; Jiang, Q. A Dynamic Series Voltage Compensator for the Mitigation of LCC-HVDC Commutation Failure. *IEEE Trans. Power Deliv.* **2021**, *36*, 3977–3987. [CrossRef]
15. Zeineldin, H.H.; El-Saadany, E.F.; Kazerani, M. Capacitor commutated converter using an adaptive active capacitor for HVDC system. In Proceedings of the Canadian Conference on Electrical and Computer Engineering. Toward a Caring and Humane Technology (CCECE 2003), Montreal, QC, Canada, 4–7 May 2003; Volume 1, pp. 529–534.
16. Tanaka, T.; Nakazato, M.; Funabiki, S. A new approach to the capacitor-commutated converter for HVDC-a combined commutation capacitor of active and passive capacitors. In Proceedings of the 2001 IEEE Power Engineering Society Winter Meeting, Columbus, OH, USA, 28 January–1 February 2001; Volume 2, pp. 968–973.
17. Guo, C.; Yang, Z.; Jiang, B.; Zhao, C. An Evolved Capacitor-Commutated Converter Embedded With Antiparallel Thyristors Based Dual-Direc-tional Full-Bridge Module. *IEEE Trans. Power Deliv.* **2018**, *33*, 928–937. [CrossRef]
18. Guo, C.; Liu, B.; Zhao, C. Improved Coordinated Control Approach for Evolved CCC-HVDC System to Enhance Mitigation Effect of Commutation Failure. *J. Mod. Power Syst. Clean Energy* **2021**, *9*, 338–346. [CrossRef]

19. Xue, Y.; Zhang, X.; Yang, C. Commutation Failure Elimination of LCC HVDC Systems Using Thyristor-Based Controllable Capacitors. *IEEE Trans. Power Deliv.* **2018**, *33*, 1448–1458. [CrossRef]
20. Kaur, J.; Chaudhuri, N. A Coordinating Control for Hybrid HVDC Systems in Weak Grid. *IEEE Trans. Ind. Electron.* **2019**, *66*, 8284–8295. [CrossRef]
21. Zhu, Y.; Zhang, S.; Liu, D.; Zhu, L.; Zou, S.; Yu, S.; Sun, Y. Prevention and mitigation of high-voltage direct current commutation failures: A review and future directions. *IET Gener. Transm. Distrib.* **2019**, *13*, 5449–5456. [CrossRef]
22. Xue, Y.; Zhang, X.; Yang, C. Series Capacitor Compensated AC Filterless Flexible LCC HVDC With Enhanced Power Transfer Under Unbalanced Faults. *IEEE Trans. Power Syst.* **2019**, *34*, 3069–3080. [CrossRef]
23. Meisingset, M. Application of Capacitor Commutated Converters in Multi-Infeed HVDC-Schemes. Ph.D. Thesis, University of Manitoba, Winnipeg, MB, Canada, 2000.
24. Yang, F.; Chang, Y. Study on Capacitor Commutated Converter applied in HVDC projects. In Proceedings of the 2007 IEEE Power Engineering Society General Meeting, Tampa, FL, USA, 24–28 June 2007; pp. 1–5.
25. Björklund, P.E.; Jonsson, T. Capacitor commutated converters for HVDC systems. *ABB Rev.* **1997**, *2*, 25–33.
26. Sadek, K.; Pereira, M.; Brandt, D.P.; Gole, A. Capacitor commutated converter circuit configurations for DC transmission. *IEEE Trans. Power Deliv.* **1998**, *13*, 1257–1264. [CrossRef]
27. Zhang, Y.; Yan, W.; Zhu, L. Tap change control of converter transformers for hybrid AC/DC power transmission systems. *Electr. Power* **2008**, *4*, 20–24.